ADVANCES IN ATMOSPHERIC SCIENCES, VOL. 37, DECEMBER 2020, 1310–1322

• **Original Paper** •

Optical, Radiative and Chemical Characteristics of Aerosol in Changsha City, Central China

Xiaoyan WU[1,2], Jinyuan XIN[*2,3,4], Wenyu ZHANG[*1], Chongshui GONG[2], Yining MA[1,2], Yongjing MA[1,2], Tianxue WEN[2], Zirui LIU[2], Shili TIAN[2], Yuesi WANG[2], and Fangkun WU[2]

[1]*College of Atmospheric Sciences, Key Laboratory of Arid Climatic Change and Reducing Disaster of Gansu Province, Lanzhou University, Lanzhou* 730000, *China*

[2]*State Key Laboratory of Atmospheric Boundary Layer Physics and Atmospheric Chemistry, Institute of Atmospheric Physics, Chinese Academy of Sciences, Beijing* 100029, *China*

[3]*University of Chinese Academy of Sciences, Beijing* 100049, *China*

[4]*Collaborative Innovation Center on Forecast and Evaluation of Meteorological Disasters, Nanjing University of Information Science & Technology, Nanjing* 210044, *China*

(Received 19 March 2020; revised 14 August 2020; accepted 21 August 2020)

ABSTRACT

Industrial pollution has a significant effect on aerosol properties in Changsha City, a typical city of central China. Therefore, year-round measurements of aerosol optical, radiative and chemical properties from 2012 to 2014 at an urban site in Changsha were analyzed. During the observation period, the energy structure was continuously optimized, which was characterized by the reduction of coal combustion. The aerosol properties have obvious seasonal variations. The seasonal average aerosol optical depth (AOD) at 500 nm ranged from 0.49 to 1.00, single scattering albedo (SSA) ranged from 0.93 to 0.97, and aerosol radiative forcing at the top of the atmosphere (TOA) ranged from −24.0 to 3.8 W m^{-2}. The chemical components also showed seasonal variations. Meanwhile, the scattering aerosol, such as organic carbon, SO_4^{2-}, NO_3^-, and NH_4^+ showed a decrease, and elemental carbon increased. Compared with observation in winter 2012, AOD and TOA decreased by 0.14 and −1.49 W m^{-2} in winter 2014. The scattering components, SO_4^{2-}, NO_3^- and NH_4^+, decreased by 12.8 μg m^{-3} (56.8%), 9.2 μg m^{-3} (48.8%) and 6.4 μg m^{-3} (45.2%), respectively. The atmospheric visibility and pollution diffusion conditions improved. The extinction and radiative forcing of aerosol were significantly controlled by the scattering aerosol. The results indicate that Changsha is an industrial city with strong scattering aerosol. The energy structure optimization had a marked effect on controlling pollution, especially in winter (strong scattering aerosol).

Key words: aerosol, optical properties, radiative forcing, chemical composition

Citation: Wu, X. Y., and Coauthors, 2020: Optical, radiative and chemical characteristics of aerosol in Changsha City, central China. *Adv. Atmos. Sci.*, **37**(12), 1310−1322, https://doi.org/10.1007/s00376-020-0076-9.

Article Highlights:

- High-concentration industrial aerosol strongly cooled the atmosphere–surface system.
- Inorganic ions and carbonaceous aerosol were the main constituents of particulate matter.
- Extinction and radiative forcing of aerosol were significantly controlled by the scattering aerosol.
- Adjustment of the energy structure played a clear role in the control of atmospheric pollution.

1. Introduction

Aerosols affect many physical and chemical processes in the atmosphere, and further impact upon weather and climate changes. Aerosol particles prevent radiation from reaching the ground through scattering or absorption. In addition, the scattering and absorption of solar radiation affect visibility. Moreover, aerosol particles can be retained in the human respiratory tract, even deep in the lungs. This directly affects human health and living environments (Charlson et al., 1992; Kaufman, 1993; Lohmann and Feichter, 2005; Wang et al., 2001; Mukai et al., 2006; Carslaw et al., 2010; Logan et al., 2013, 2014; Reisen et al., 2013; Sheng et al., 2013; Chen et al., 2014; IPCC 2014; Xin et al., 2015; Ma et al., 2016). Meanwhile, chemical composi-

* Corresponding authors: Jinyuan XIN, Wenyu ZHANG
Email: xjy@mail.iap.ac.cn, zhangwy@lzu.edu.cn

tions in different regions vary greatly because of different emissions, and show different radiative effects. Generally speaking, anthropogenic aerosols such as sulfate and nitrate have strong scattering characteristics and mainly exhibit cooling effects; black carbon shows clear heating effects owing to strong absorption characteristics; sea salt, which is a natural aerosol, exhibits heating effects; and dust aerosol exhibits strong heating effects in the shortwave range and cooling effects in the longwave range (Qian et al., 1998; Jacobson, 2002; Zhang et al., 2002, 2008; Che et al., 2009; Li et al., 2009; Wang et al., 2010; Singh and Dey, 2012; Xu et al., 2013; Koepke et al., 2015; Huang, 2016; Tian et al., 2016; Zhang and Liao, 2016). As one of the world's heavily polluted regions, China has a major impact on global climate change and human health. However, there are huge differences in the physical and chemical characteristics of atmospheric particles at different types of sites in different regions of China (Wang et al., 2001; Xin et al., 2007, 2015, 2016a, b; Zhang et al., 2012, 2019; Zhao et al., 2013a, b; Tian et al., 2016; Cao et al., 2016; Huang, 2016). Therefore, it is necessary to study the optical, radiative and chemical properties of aerosol and understand the relationships among them, which is also helpful for pollution control.

There have been many studies in China that have concentrated on the country's industrially developed and heavily polluted areas, such as the Beijing–Tianjin–Hebei region, the Yangtze River Delta region, and the Pearl River Delta region (Zheng et al., 2005; Zhao et al., 2013a, b, 2015, 2018; Gong et al., 2014; Kong et al., 2014, 2017; Shao et al., 2017; Tang et al., 2018; Zhang et al., 2018). Currently, we know that the aerosol optical depth (AOD) is relatively large in central and southeastern China. Furthermore, there are large quantities of anthropogenic aerosol emissions in the southeast, so many areas in eastern China have shown the presence of contaminants and mixed mineral and smoke aerosols (Xin et al., 2007, 2015, 2016a; Che et al., 2009, 2015). However, few researchers have focused on central China, despite the extinction effect of aerosol being strong there. Central China (including Henan, Hubei and Hunan provinces) includes the middle reaches of the Yellow River and Yangtze River. It is surrounded by the Beijing–Tianjin–Hebei region, the Yangtze River Delta, the Pearl River Delta, the Sichuan Basin, and the Guanzhong Plain, and connects the entire country. Previous research showed that the average AOD in central China was 0.61 between 2003 and 2012, which was higher than that in North China (0.57) and the Pearl River Delta (0.41) (Chen, 2014). Furthermore, the AOD at 500 nm in Wuhan was approximately 0.88, 1.07, 1.11, 1.38, 1.02, 0.92 and 1.07 for the years 2007, 2008, 2009, 2010, 2011, 2012 and 2013, respectively, which were slightly higher than the values in Beijing during 2002–07 (0.79, 0.75, 0.85, 0.74, 0.86 and 1.06, respectively). The annual mean Ångström exponent (AE) was approximately 1.22, which showed the dominance of fine particle pollution. The monthly variation of single scattering albedo (SSA) was closely related to the hygroscopic growth of aerosols, fossil fuels and biomass burning (Wang et al., 2015; Zhang et al., 2015). The annual average AOD at 440 nm in Zhengzhou was 0.89 ± 0.57 in 2008, and the AE was 1.47, which showed urban industrial aerosol particles were still the main controlling particles in Zhengzhou (Tian et al., 2010). The annual mean $PM_{2.5}$ in Zhengzhou was 191, 185 and 150 μg m^{-3} in 2013, 2014 and 2015, which were higher than the average in the Yangtze River Delta (59.7 μg m^{-3}) (Jiang et al., 2018). The annual average concentration of $PM_{2.5}$ was 82.81 μg m^{-3} in 2013 and 76.38 μg m^{-3} in 2014 in Changsha; the corresponding pollution day ratios ($PM_{2.5}$ > 75 μg m^{-3}) were 44.11% and 39.45% (Wang, 2016). The annual mean AOD and AE were 0.95 ± 0.52 and 1.06 ± 0.31 from 2012 to 2013 (Xin et al., 2015). The annual average concentration of PM_{10} had been in steady decline in China during 2004–12. However, PM_{10} showed a large increase in almost all regions in 2013. Overall, we can see that central China is a highly polluted area, and there have not been many studies that have analyzed in depth the properties of aerosols in central China. Therefore, studying the properties of aerosols in central China has significance.

Changsha is an important central city in the middle reaches of the Yangtze River. Its location is (27.81°–28.68°N, 111.88°–114.25°E) in the north of Hunan Province and the middle of Xiangjiang Valley. Its unique geography and topography make it difficult for air pollutants to spread, thus affecting the environmental quality in Changsha. In addition, Changsha–Zhuzhou–Xiangtan forms a triangular industrial zone, so the atmosphere may also be affected by atmospheric pollutants emitted by other cities in this zone. The long-term coal-based energy structure causes soot-type pollution, with SO_2 and NO_2 as the main pollutants. At the same time, dust is also a major pollutant (Changsha Municipal Bureau of Statistics, and Changsha investigation team of National Bureau of Statistics, 2018). Furthermore, Changsha was in the process of an energy structure adjustment during 2012–14. Therefore, we studied the optical, radiative and chemical properties of aerosol in Changsha during 2012–14 and report the results in this paper. In our research, we analyzed the seasonal variations of optical properties (AOD, AE), radiative properties (SSA, radiative forcing) and chemical properties [organic carbon (OC), elemental carbon (EC), water-soluble ions] in Changsha during 2012–14. Meanwhile, we compared the changes during the three years. Then, we performed a backward trajectory analysis and potential source area analysis to understand the impacts of airmass transmission. Lastly, we studied the relationships among the optical, radiative and chemical properties.

2. Data and methods

Changsha station (28.2°N, 113.067°E) of the CARE-China network is located in the east of Changsha, at an altitude of 58 m. It represents a typical urban station influenced by intensive human activities. The geographical location of Changsha Station and the distribution of AOD monitored by MODIS over central China during 2012–14 is shown in Fig. 1. We can see that Changsha is in the pol-

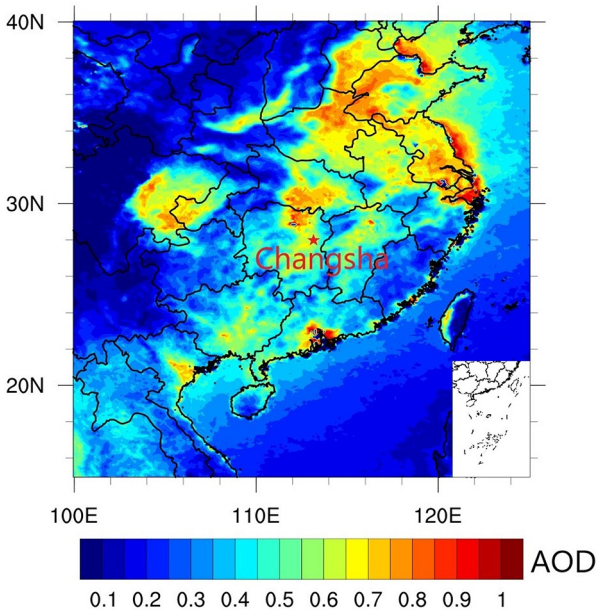

Fig. 1. Geographical location of Changsha station and the distribution of AOD monitored by MODIS over central China from 2012 to 2014.

luted area.

In this study, the basic optical parameter, AOD, was observed by a Microtops II solar photometer, manufactured by Solar Light, USA. The photometer has five spectral channels: 440 nm, 500 nm, 675 nm, 870 nm and 936 nm. All the channels can be used to determine AOD according to the Lambert–Beer law. AE, representing the size of aerosol particles, was calculated along with the AOD in three channels: 440 nm, 500 nm and 675 nm. SSA and values of radiative forcing at the top of the atmosphere (TOA), in the atmosphere (ATM), and at the bottom of the atmosphere (SFC), were calculated by the Santa Barbara DISORT Atmospheric Radiative Transfer (SBDART) software. We chose the midlatitude atmospheric profile in SBDART. The input consisted of the aerosol parameters, including AOD, SSA, asymmetric parameters and AE, and surface albedo of MODIS. The results were combined with MODIS observations. More detailed descriptions can be found in our previous papers (Gong, 2014; Xin et al., 2016b; Gong et al., 2017). SSA represents the ratio of aerosol scattering to its total extinction (scattering plus absorption) (Xia et al., 2013; Gong, 2014; Koo et al., 2016; Ram et al., 2016; Gong et al., 2017; Palancar et al., 2017). The AOD and SSA data mentioned in this paper are all 500 nm results. The calculated results were under clear-sky conditions, and the relevant effects of the cloud layer on the results were not considered in this study. The absorption aerosol optical depth (AAOD) and scattering aerosol optical depth (SAOD), respectively indicating the degree of aerosol absorption and scattering, were calculated with the AOD and SSA [AAOD = (1 − SSA) × AOD; SAOD = SSA × AOD)] (Zhao et al., 2018). Additionally, meteorological data were provided by the China Meteorological Data Network (http://www.nmic.cn/), including daily average data such as relative humidity (RH), wind speed, wind direction, etc.

The mass concentration of $PM_{2.5}$ was obtained with an online atmospheric particulate matter monitoring system (TEOM 1400a) based on a tapered element oscillating microbalance. The $PM_{2.5}$ data were output every minute. The atmospheric particulate matter was collected using an Anderson impact grading sampler (Series 20-800 Mark II), manufactured by American Thermoelectric Corporation, to study the concentration and spectral distribution of chemical compositions. $PM_{2.1}$, obtained by Anderson sampling, is significantly linearly correlated ($R^2 = 0.89$, $p < 0.05$) with online $PM_{2.5}$ (Tian et al., 2016). The atmospheric particulate matter was divided into nine particle size segments: < 0.43 μm, 0.43–0.65 μm, 0.65–1.1 μm, 1.1–2.1 μm, 2.1–3.3 μm, 3.3–4.7 μm, 4.7–5.8 μm, 5.8–9.0 μm, and > 9.0 μm. The sampling frequency was one sampling per week and collected continuously for 48 h each time. The water-soluble ions were analyzed by ion chromatography (Dionex ICS-90, United States) and a thermal/optical carbon analyzer (DRI Model 2001A, Desert Research Institute, United States) was used to determine EC and OC (Tian et al., 2016; Su, 2018). The analysis method of the thermal/optical carbon analyzer adopts IMPROVE_A. Furthermore, we used the EC tracer method to estimate the mass concentration of secondary organic carbon (SOC) and primary organic carbon (POC) [$SOC = OC_{tot} - (OC / EC)_{pri} \times EC$; $POC = (OC / EC)_{pri} \times EC$] (Hu et al., 2016). We also estimated the organic matter (OM) through the equation OM = 1.4 × OC (Srinivas and Sarin, 2014).

We employed the TrajStat (Trajectory Statistics) model for seasonal backward trajectory clustering. The TrajStat model is software developed by NOAA HYSPLIT users, using the same trajectory calculation module as HYSPLIT (Wang et al., 2009). The endpoint of the trajectory was Changsha station, and the backward time was 72 h. Meanwhile, we computed the potential source contribution function and concentration weighted trajectory analyses according to the $PM_{2.5}$ data. The meteorological data input was from the NCEP reanalysis dataset from NOAA.

3. Results and discussion

3.1. *Basic properties of aerosol*

Figure 2 presents the seasonal mean changes of wind speed, RH, $PM_{2.5}$, AE and AOD between 2012 and 2014. Wind speed varied from 1.6 m s^{-1} to 2.3 m s^{-1} in Changsha. It was large in summer 2013, corresponding to a low $PM_{2.5}$ and AOD. More details are given in Fig. S1 (in the Electronic Supplementary Material, ESM). The seasonal RH varied from 58% to 81% in Changsha, providing enough water vapor for atmospheric reactions. The annual $PM_{2.5}$ was 77.8 ± 27.4 μg m^{-3} (shown in Table S1 in the ESM), which was more than in Beijing (66 ± 54 μg m^{-3}), Shenyang (71 ± 55 μg m^{-3}) from 2012 to 2013 (Xin et al., 2016a). $PM_{2.5}$ was obviously higher in winter and lower in summer, ran-

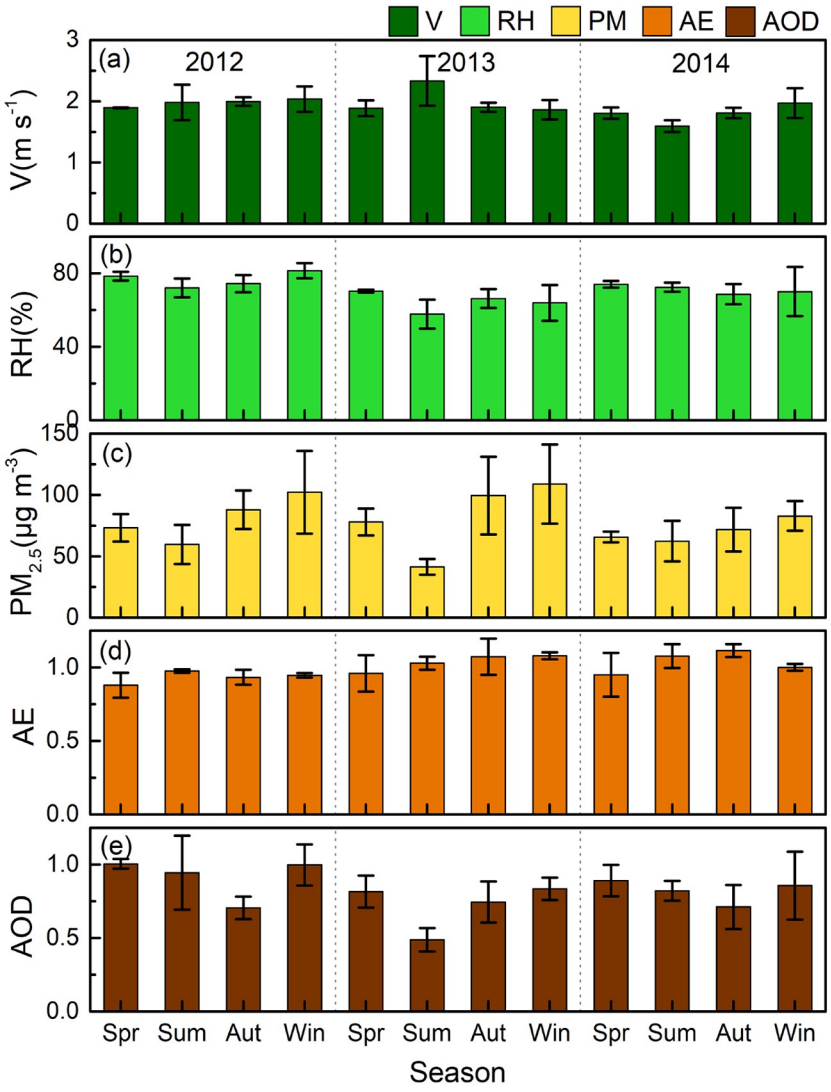

Fig. 2. Seasonal means of wind speed (V), RH, mass concentration of fine particles ($PM_{2.5}$), AE and AOD during the observation period (2012–14) at Changsha station. The bars represent the seasonal means of each parameter, and the black error bars are the standard deviations of seasonal means calculated by monthly values.

ging from 41.4 μg m^{-3} to 108.9 μg m^{-3} in its seasonal means. Besides, the mass concentration of $PM_{2.5}$ in winter 2014 decreased by 19.4 μg m^{-3} (19.0%) compared with winter 2012. The annual average AOD and AE were 0.81 ± 0.19 and 1.00 ± 0.11, respectively (Table S1). The annual AOD value was almost the same as those of other industrial cities, such as Shenyang (0.61 ± 0.13), Tangshan (0.80 ± 0.26) and Lanzhou (0.74) (Gong et al., 2017; Zhang et al., 2018; Zhao et al., 2018). We therefore know that it had similar aerosol properties as these industrial cities. In terms of the three-year average, AOD had larger values in spring and winter (~0.90), while AE showed smaller values (0.93) in spring, which was identical to the results in Zhengzhou (Tian et al., 2010). However, this seasonal change was different to observation around the Bohai Rim, such as in Beijing and Tangshan, which followed the order summer > spring > autumn > winter (Zhang et al., 2018). In 2012–14, AOD had a similar seasonal difference. AOD was larger in winter and spring. Compared to winter 2012, AOD decreased by 0.14 in winter 2014. AE showed smaller values in spring because of dust aerosol. Also, it showed a growth trend during 2012–14. It should be noted that all the seasonal means were more than 0.75, indicating that aerosol particles in Changsha were dominated by the fine particle mode. To sum up, we have found that AOD and $PM_{2.5}$ decreased and AE overall increased during the period of energy structure optimization in Changsha.

Figure 3 shows the seasonal average changes of SSA, AAOD, SAOD and radiative forcing (TOA, ATM and SFC) from 2012 to 2014. For the three-year average, SSA values were all larger than 0.94, which showed obvious urban characteristics (Gong et al., 2017). Seasonal mean values of SSA were all greater than 0.93, which showed the scattering effect of aerosol was very strong, and manmade scattering aer-

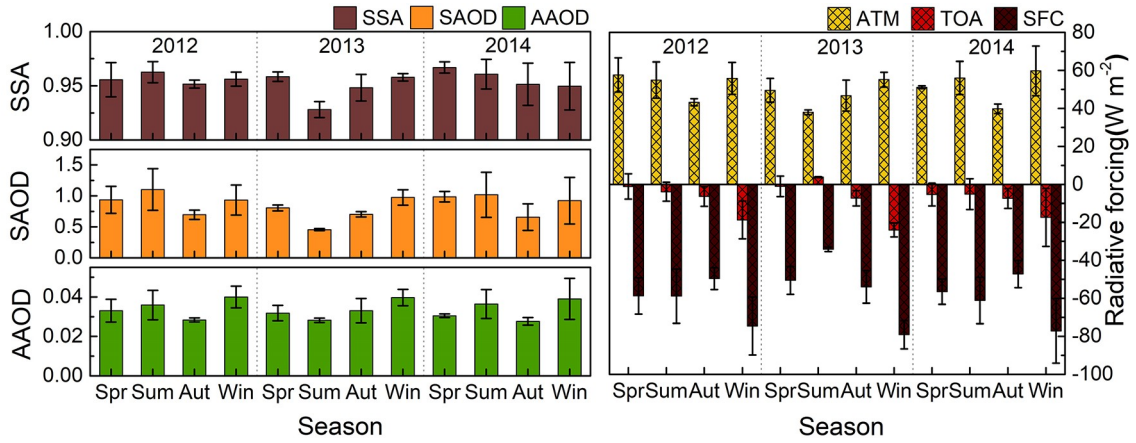

Fig. 3. Seasonal means of SSA, AAOD, SAOD and radiative forcing (TOA: top of the atmosphere; ATM: in the atmosphere; SFC: bottom of the atmosphere) during the observation period (2012–14) at Changsha station. The bars represent seasonal means of each parameter, and the black error bars are the standard deviations of seasonal means calculated by monthly values.

osol such as sulfate and nitrate was dominant in Changsha. SAOD and AAOD showed their highest values in winter due to the emissions. The overall trend of SAOD was similar to AOD. It can be seen that TOA in Changsha was basically negative, apart from in summer 2013 (3.8 W m^{-2}), ranging from −24.0 W m^{-2} to −1.1 W m^{-2}. ATM and SFC changed from 37.9 W m^{-2} to 59.8 W m^{-2} and −79.1 W m^{-2} to −34.1 W m^{-2}. All radiative forcings had their largest values in winter, and small values in summer. Furthermore, the variation of TOA was different from that in Beijing, showing the cooling effect was weaker in winter and spring and relatively stronger in summer and autumn (Gong, 2014). In summer, the scattering effect weakened because of rainfall and reduced anthropogenic aerosol emissions. Therefore, the cooling effect of aerosol was weak in summer. Correspondingly, the cooling effect was strong in winter due to more anthropogenic aerosol emissions. In the three-year trend, the cooling effect of aerosol showed a small decrease. It was related to the decrease in scattering aerosol emissions during the energy structure optimization process. This trend is expected to reduce the atmospheric stability and promote pollutant diffusion. From the results, we can see anthropogenic aerosol had a strong scattering effect in Changsha, and there might be differences in aerosol types with northern regions. The energy structure optimization measures improved diffusion conditions.

Figure 4 shows the seasonal average mass concentrations of OC, EC and water-soluble inorganic ions (SO_4^{2-}, NO_3^-, NH_4^+, Na^+, Cl^-, K^+, NO_2^-, Mg^{2+} and F^-) in nine particle size segments from 2012 to 2014 in Changsha. From the three-year average, the average of the total chemical components (including OC, EC and water-soluble inorganic ions) was higher in winter (89.3 μg m^{-3}) than in other seasons (spring: 58.5 μg m^{-3}; summer: 44.4 μg m^{-3}; autumn: 58.9 μg m^{-3}) in $PM_{2.1}$, due to the intensity of the emissions and weather conditions. The concentrations of $PM_{2.5}$ and EC, OC, SO_4^{2-}, NO_3^-, and NH_4^+ in $PM_{2.1}$ in winter were 1.8, 2.0, 1.6, 1.4, 5.9, and 2.6 times higher than those in summer (Table S1). From Fig. 4, we can see that OC was greater than EC in almost the nine particle size segments. Furthermore, OC and EC presented a bimodal distribution in 0.43–0.65 μm and 4.7–5.8 μm. EC was concentrated in $PM_{0.43}$, contributing approximately 20%–59%. The seasonal averages of OC ranged from 9.5 μg m^{-3} to 25.8 μg m^{-3} in $PM_{2.1}$, and from 5.1 μg m^{-3} to 18.9 μg m^{-3} in $PM_{2.1\text{-}100}$. Meanwhile, EC ranged from 2.0 μg m^{-3} to 7.4 μg m^{-3}, and from 0.9 μg m^{-3} to 4.1 μg m^{-3}, correspondingly (Figs. S2 and S3). Both were higher than those in Tangshan and Beijing (Zhang et al., 2018). All of the above results indicate that carbonaceous aerosol pollution was heavy. Human emissions such as coal combustion, motor vehicle exhaust and biomass combustion were significant (Seinfeld and Pandis, 1998; Kirkevåg et al., 1999; Jacobson, 2001; Cao et al., 2005; Huan et al., 2005). Furthermore, OC showed a decrease from 2012 to 2014 because of more biomass burning and less fossil fuel burning (Figs. S5 and S6). The total water-soluble ions ranged from 20.4 μg m^{-3} to 66.5 μg m^{-3} in $PM_{2.1}$. The water-soluble ions were centrally distributed in $PM_{0.43\text{-}2.1}$, contributing from 53% to 70%. Secondary inorganic ions (SIA, including SO_4^{2-}, NO_3^-, and NH_4^+), the most important water-soluble inorganic ions in atmospheric particles, accounted for 77%–92% in seasonal averages, indicating that secondary aerosol pollution played an important role in Changsha. The high SO_4^{2-} indicated that atmospheric particulate matter was affected by coal combustion in Changsha. Apart from differences in seasonal emissions, the concentrations of NO_3^- and NH_4^+ in winter were greater than those in summer, possibly because of the less extensive influence of temperature on the state of particulate matter (Russell et al., 1983; Guo et al., 2010; Cao et al., 2016). The concentration of SO_4^{2-} and NH_4^+ decreased from spring to winter in 2014. Besides, we found that OC and SO_4^{2-} had a downward trend overall. Comparing the values in winter, SIA, SO_4^{2-}, NO_3^- and NH_4^+ decreased by 28.4 μg m^{-3} (51.1%), 12.8 μg m^{-3} (56.8%), 9.2 μg m^{-3} (48.8%) and 6.4 μg m^{-3} (45.2%), respectively, from 2012 to

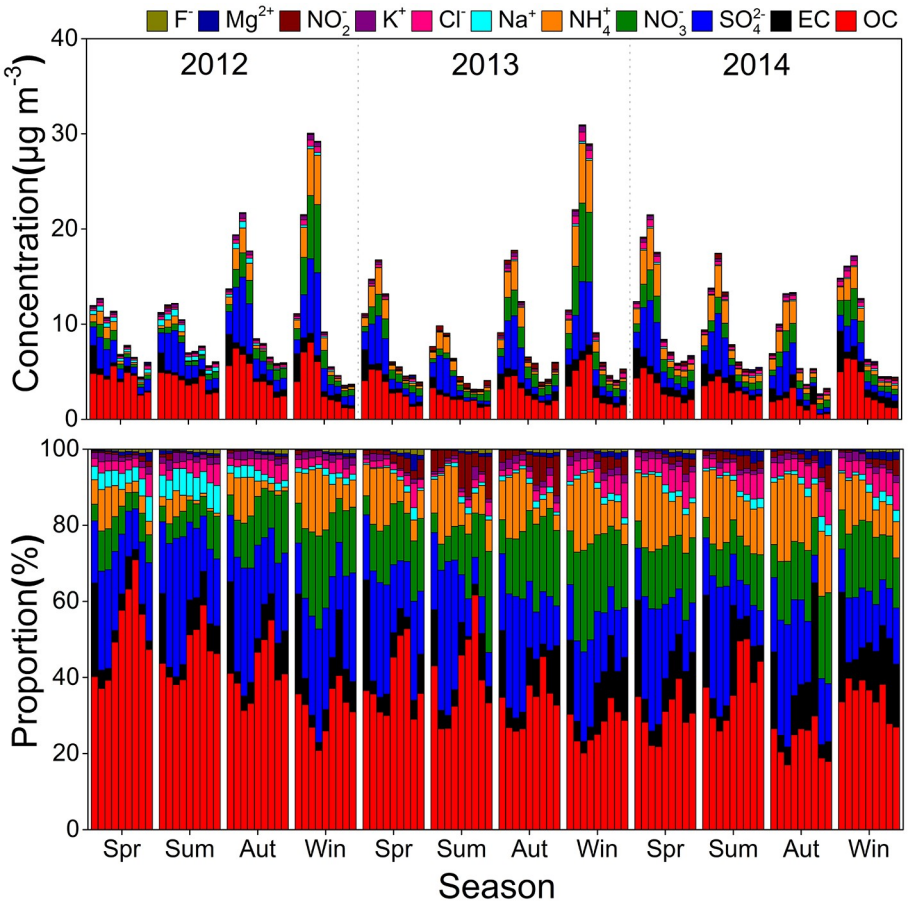

Fig. 4. Seasonal means of total chemical compositions including OC, EC and water-soluble inorganic ions and their corresponding ratios in nine particle size segments during the observation period (2012–14) at Changsha station. From left to right, the columns represent the mass concentration of chemical compositions with diameter < 0.43 μm, 0.43–0.65 μm, 0.65–1.1 μm, 1.1–2.1 μm, 2.1–3.3 μm, 3.3–4.7 μm, 4.7–5.8 μm, 5.8–9.0 μm, and > 9.0 μm.

2014. Human emissions such as fuel combustion had been reduced year by year. The energy structure was gradually optimized and the secondary pollution reduced, which is verified by Figs. S6 and S7. In Fig. S7, we can see that OM and SOM (secondary organic matter) showed a downward trend, while POM (primary organic matter) increased during 2012–14. Therefore, the mass concentrations of chemical components were high and the results showed there was serious secondary pollution in Changsha. Energy structure optimization changed the proportions of chemical components. Secondary aerosols decreased and pollution was controlled to a certain extent.

Figure 5 shows seasonal mean variations of OC/EC and NO_3^-/SO_4^{2-} in fine particle size segments (< 0.43 μm, 0.43–0.65 μm, 0.65–1.1 μm and 1.1–2.1 μm) from 2012 to 2014 in Changsha. In this paper, we use the ratio of OC/EC to initially determine the source of carbonaceous aerosols (Ram and Sarin, 2010) and the ratio of NO_3^-/SO_4^{2-} to compare the contribution of fixed sources (such as coal) and mobile sources (such as motor vehicles) to particulate matter in the atmosphere (Watson et al., 1994; Huang et al., 2014; Su et al., 2018). It can be seen from Fig. 5 that the OC/EC values were generally greater than 2.0, apart from the < 0.43 particle size segment, which showed it was mainly based on SOC emissions in Changsha. In $PM_{0.43}$, the percentage of OC/EC < 2 was 75%, showing that POC was dominant in this particle size segment. The OC/EC values ranged from 1.1 to 19.3 in fine modes, which indicated that coal-fire emissions and biomass-burning emissions existed (Jiang, 2017). The ratio of OC/EC had obvious seasonal changes, with a larger value in summer and a smaller value in winter. The low temperature in winter caused photochemical reactions to weaken, so OC/EC was generally lower in winter than in summer (Pio et al., 2011). Also, the type of pollutant and plant discharge contributed to this result. There were active plant emissions with more OC in summer and more coal combustion in winter. We guessed there was a lot of biomass burning so the values of OC/EC were high in 2012, as indicated by the fire point data in Fig. S5. From the three-year trend, it can be seen that OC had decreased, EC had increased, and the OC/EC values showed a decline. This phenomenon illustrated that secondary emissions had been controlled. The ratio of NO_3^-/SO_4^{2-} had obvious seasonal changes, with the highest in winter and lowest in sum-

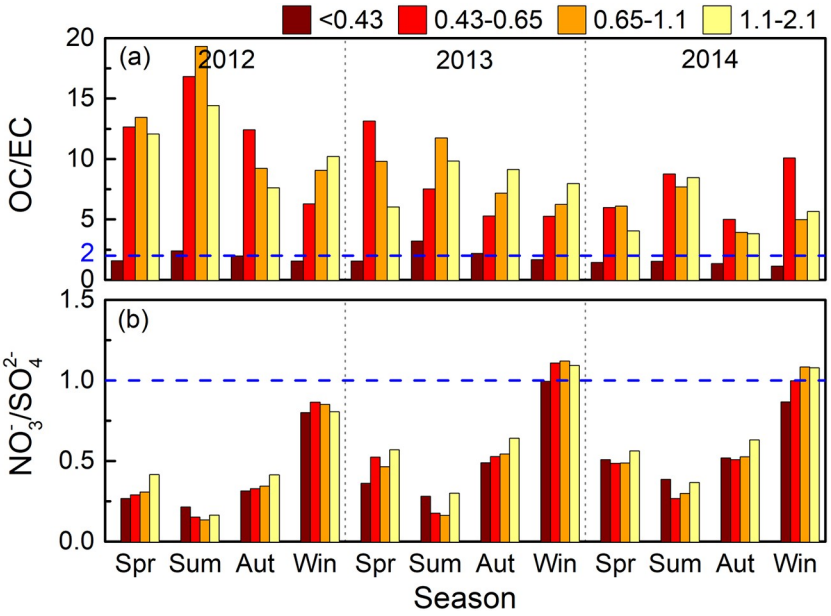

Fig. 5. Seasonal mean variations of (a) OC/EC and (b) NO_3^-/SO_4^{2-} in fine particle size segments during the observation period (2012–14) at Changsha station. From left to right, the columns represent the values with diameter < 0.43 μm, 0.43–0.65 μm, 0.65–1.1 μm and 1.1–2.1 μm. The blue dotted line represents a critical value: it means that SOC occupies the main role when OC/EC > 2; on the contrary, the POC occupies the main role in (a); the contribution of fixed sources (such as coal) is more than that of mobile sources (such as motor vehicles) when $NO_3^-/SO_4^{2-} < 1$ in (b).

mer, followed by spring and autumn. The values of NO_3^-/SO_4^{2-} were mostly lower than 1, which showed coal still played a leading role in the energy structure and fixed sources dominated over mobile sources. Meanwhile, the overall trend has risen because the energy structure was continuously optimized and fossil energy consumption continued to decrease (Fig. S6). The ratios in coarse modes had a contrasting trend (Fig. S3): high in summer and low in winter, and it was almost all greater than 1, showing that the contribution of the moving sources in the coarse mode was large. A possible reason is that nitric acid gas could be adsorbed by coarse particles to form NO_3^-, and SO_4^{2-} reacted with cloud droplets or droplets when the RH was high (Huang et al., 2013; Cao et al., 2016).

To sum up, there were clear industrial aerosol characteristics with strong scattering effects in Changsha. Coal consumption reduced and natural gas consumption increased during the energy structure optimizing process from 2012 to 2014. Besides, AOD, particle matter and radiative forcing were decreased. The extinction of aerosol declined and the visibility improved. TOA expressed a weaker cooling effect and pollutant diffusion conditions improved. AE showed an increasing trend while coarse particles were firstly controlled during the pollution control process. The degree of change in each component was not consistent. The mass concentrations of SO_4^{2-}, NO_3^-, NH_4^+ and OC decreased in autumn and winter, while EC increased. Comparing the results of optical, radiative and chemical properties of aerosol, we found that, with the energy structure optimization and the control measure from the government, chemical compositions changed, while the extinction and radiative forcing of aerosol decreased with it. Anthropogenic emissions, such as fossil fuels and secondary aerosol, reduced, and there was improvement in pollution control.

3.2. *Backward trajectory and potential source area analysis*

Figure 6 represents the backward trajectories of aerosol in the four seasons, as well as meteorological factors and optical, physical and chemical properties of aerosol corresponding to each trajectory. The route and direction of the trajectory indicates the area where the air mass passed before reaching the observation site. From Fig. 6a, the clustering results of the backward trajectories in spring consisted of four categories, three of which [Type-I (21%), Type-II (37%), Type III (29%)] moved slowly and polluted more seriously, for which $PM_{2.5}$ was 77.96 μg m^{-3}, 72.77 μg m^{-3} and 83.47 μg m^{-3}. Type-IV (13%) originated from marine air masses. Correspondingly, the concentrations of all chemical compositions and $PM_{2.5}$ (45.10 μg m^{-3}) were lower and AOD was smaller than for the others. The clustering results were classified into six categories in summer (Fig. 6b), which could be divided into two categories, according to the direction: south (52%) and north (48%). It can be seen that the concentrations of chemical compositions and $PM_{2.5}$ originating from the southern air mass (Type-II, Type-III and Type-V) were low, and AOD was also small. Furthermore, TOA and SFC exhibited weak cooling effects because of

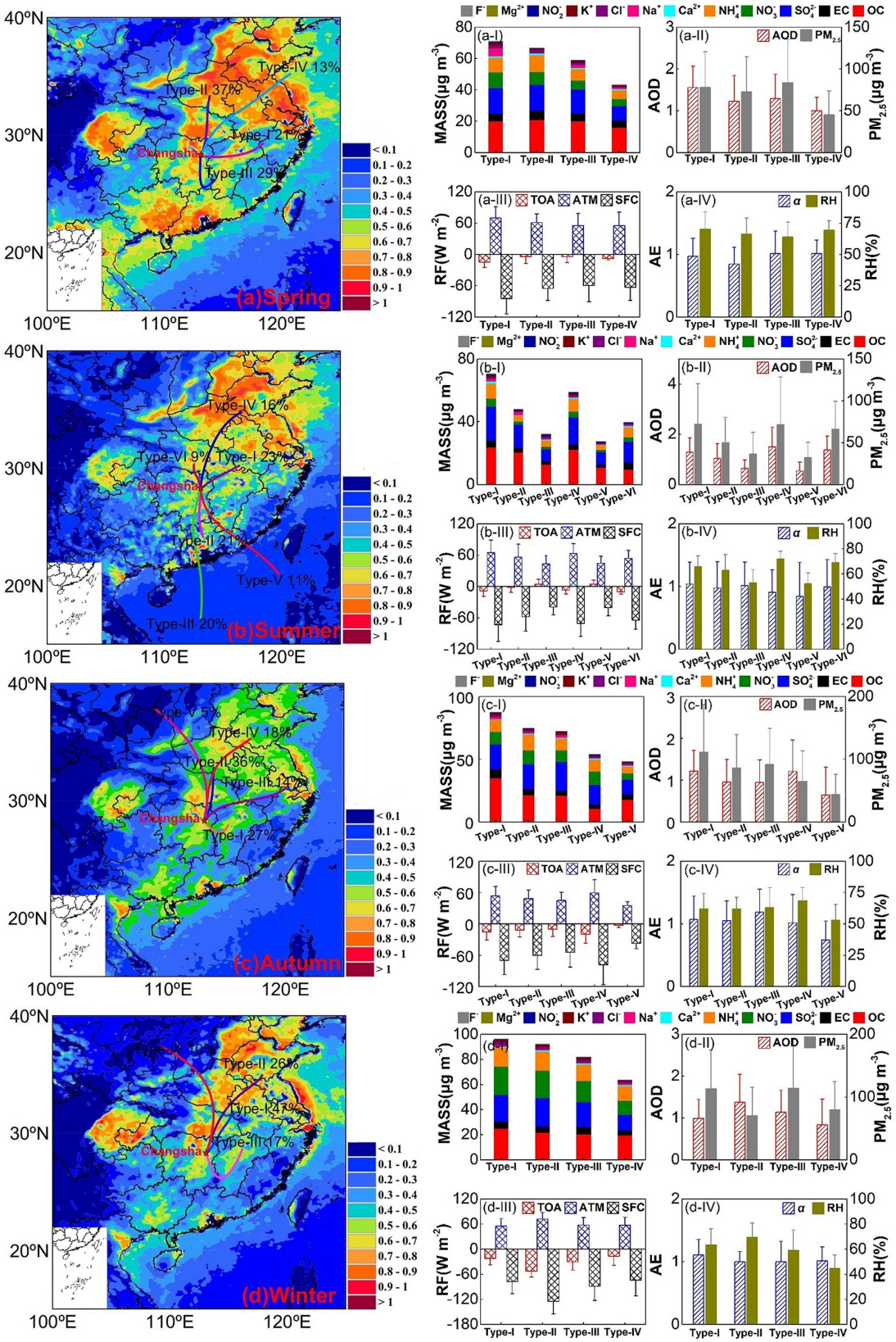

Fig. 6. Backward trajectory clustering and characteristics and meteorological factors of aerosols under different trajectory types in (a) spring, (b) summer, (c) autumn and (d) winter. The mass concentration of chemical compositions including water-soluble inorganic ions, EC, and OC in $PM_{2.1}$ in (Ⅰ), AOD and the mass concentration of $PM_{2.5}$ in (Ⅱ), radiative forcing at the top of the atmosphere (TOA), in the atmosphere (ATM) and at the surface (SFC) in (Ⅲ), AE (α) and RH in (Ⅳ).

the wet and clean air mass from the south with less anthropogenic scattering aerosols. The clustering results in autumn shown in Fig. 6c consisted of five categories: Type-I, Type-II, Type-III and Type-IV, which were derived from the northeast, while Type-V (5%) was from the northwest. The RH of the Type-V air mass, the concentration of SIA and $PM_{2.5}$ were lower than for others, as well as the AOD and AE, indicating that the northwest region transmitted dry, coarse-mode particles and less of an effect of anthropogenic aerosols. Other than this, the cooling effect of TOA was smaller because of natural aerosol such as dust. The clustering results in winter are shown in Fig. 6d, and are similar to the direction in autumn, from the northeast (90%) and northwest (10%). The properties of the air mass in winter originating from the northwest were similar to those in autumn, but its corresponding AE was greater than 1, indicating fine-mode particles were dominant in winter. From the results of the backward trajectory and the potential source area (Fig. S8), it is easy to see that the atmospheric pollution in Changsha was greatly affected by local pollution as well as airmass transportation in neighboring provinces and cities. These caused high concentrations of $PM_{2.5}$ and high AOD in Changsha. Meanwhile, the air mass from the ocean or northwest would improve diffusion conditions and weaken air pollution. Therefore, governing local pollution in Changsha is an effective method. Collaboration across regions is also important.

3.3. *Relationship between optical, radiative and chemical properties*

Figure 7 shows the relationship between AOD, $PM_{2.5}$, SSA, TOA and chemical components in terms of their seasonal means. Also, the colorbar presents the RH because of the hygroscopic growth of aerosols. As $PM_{2.5}$ increased, AOD showed an increase and TOA a stronger cooling effect. Meanwhile, with the increase of OM and SIA, TOA showed a decrease. It is well known that when the mass concentrations of $PM_{2.5}$ increase, the ratio of anthropogenic aerosol emissions will increase in urban cities and aerosol will display larger extinction, stronger scattering effects and cooling effects. All chemical compositions worked together on optical and radiative properties. The degree of optical and radiative changes caused by different compositions was different. In autumn and winter, chemical compositions had a more pronounced effect on AOD and TOA because of anthropogenic aerosol emissions and poor meteorological diffusion conditions. Besides, the hygroscopic growth of aerosols would affect aerosol properties. Thus, there are some discrete points in Fig. 7. Some of the time, although OM was not large, TOA exhibited a strong cooling effect with the large SIA. Therefore, the scattering aerosols played an important role in aerosol direct radiative forcing. Overall, $PM_{2.5}$ made an important contribution to AOD and TOA. Meanwhile, SIA was the important component of $PM_{2.5}$. Furthermore, controlling SIA components in $PM_{2.5}$ remains an important step in controlling the atmospheric aerosol pollution.

4. Conclusions

By analyzing the optical, physical and chemical properties of aerosol in Changsha, obvious industrial pollution characteristics were found. Overall, AOD showed large values in spring and winter, while there was a downward trend. AE indicated that aerosol particles mainly existed as fine-mode, and coarse-mode particles reduced. SSA were all more than 0.90 and the radiative forcing was almost negative, indicating that they were dominated by anthropogenic scattering aerosols. OC and EC generated by human emissions and secondary emissions were greater. OC and SOM showed a down-

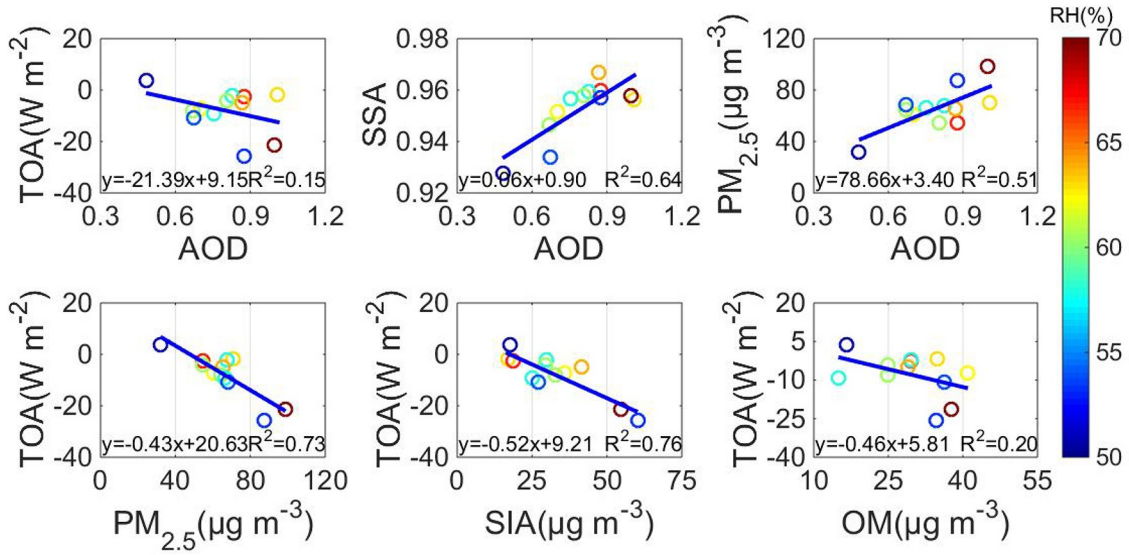

Fig. 7. Relationship between optical, radiative and chemical properties in seasonal averages during the observation period (2012–14) at Changsha station. The blue line is the fitted straight line from least-squares. The color scale represents the RH, the blue circles in the lower RHs, while the red circles in the higher RHs.

ward trend. The average concentration of total water-soluble ions was highest in winter, while SIA (including SO_4^{2-}, NO_3^- and NH_4^+) was the main constituent in atmospheric particles. Coal combustion still played a leading role in the energy structure, as indicated by the higher concentrations of SO_4^{2-} than NO_3^-. The extinction and radiative forcing of aerosol was significantly controlled by chemical compositions apart from the mass concentration of particulate matter. Besides, SIA was the important component affecting optical and radiative properties. Chemical components decreased in winter and caused lower AOD and weaker cooling effects during the energy structure optimization. SIA decreased by 51.1% and AOD by 14.2%. The backward trajectories and the potential source area indicated that the atmosphere in Changsha was affected by local pollution and neighboring provinces and cities. Governing local pollution in Changsha is an effective method.

In summary, Changsha was greatly affected by industrial aerosol with strong scattering effects. Atmospheric visibility improved and pollution was controlled to some extent during the energy structure optimization process from 2012–14. Further control of local anthropogenic pollution is still necessary.

Acknowledgements. This study was supported by the National Key Research and Development Program of China (Grant No. 2016YFC0202001), the Chinese Academy of Sciences Strategic Priority Research Program(Grant No. XDA23020301), and the National Natural Science Foundation of China (Grant Nos. 42061130215 and 41605119). The authors are grateful for the MODIS services provided by the NASA EOSDIS Land Processes Distributed Active Archive Center (LP DAAC). Researchers are welcome to email the Corresponding Author (Prof. Jinyuan XIN: xjy@mail.iap.ac.cn) and share the data in manuscript by a bilateral cooperation.

Electronic supplementary material: Supplementary material is available in the online version of this article at https://doi.org/10.1007/s00376-020-0076-9.

REFERENCES

Cao, J. J., and Coauthors, 2005: Characterization and source apportionment of atmospheric organic and elemental carbon during fall and winter of 2003 in Xi'an, China. *Atmospheric Chemistry and Physics*, **5**(11), 3127–3137, https://doi.org/10.5194/acp-5-3127-2005.

Cao, S., D. Wu, L. Z. Chen, J. R. Xia, J. G. Lu, G. Liu, F. Y. Li, and M. Yang, 2016: Characteristics of water-soluble inorganic ions of aerosol in China: A review. *Environmental Science & Technology*, **39**(8), 103–115, https://doi.org/10.3969/j.issn.1003-6504.2016.08.018. (in Chinese with English abstract)

Carslaw, K. S., O. Boucher, D. V. Spracklen, G. W. Mann, J. G. L. Rae, S. Woodward, and M. Kulmala, 2010: A review of natural aerosol interactions and feedbacks within the Earth system. *Atmospheric Chemistry and Physics*, **10**, 1701–1737, https://doi.org/10.5194/acp-10-1701-2010.

Changsha Municipal Bureau of Statistics, and Changsha investigation team of National Bureau of Statistics, 2018: *Changsha Statistical Yearbook*. China Statistics Press, Beijing. (in Chinese)

Charlson, R. J., S. E. Schwartz, J. M. Hales, R. D. Cess, J. A. Coakley Jr., J. E. Hansen, and D. J. Hofmann, 1992: Climate forcing by anthropogenic aerosols. *Sciences*, **255**(5043), 423–430, https://doi.org/10.1126/science.255.5043.423.

Che, H., and Coauthors, 2015: Ground-based aerosol climatology of China: Aerosol optical depths from the China aerosol remote sensing network (CARSNET) 2002-2013. *Atmospheric Chemistry and Physics*, **15**(13), 7619–7652, https://doi.org/10.5194/acp-15-7619-2015.

Che, H. Z., Z. F. Yang, X. Y. Zhang, C. Z. Zhu, Q. L. Ma, H. G. Zhou, and P. Wang, 2009: Study on the aerosol optical properties and their relationship with aerosol chemical compositions over three regional background stations in China. *Atmos. Environ.*, **43**(5), 1093–1099, https://doi.org/10.1016/j.atmosenv.2008.11.010.

Chen, J. S., J. Y. Xin, J. L. An, Y. S. Wang, Z. R. Liu, N. Chao, and Z. Meng, 2014: Observation of aerosol optical properties and particulate pollution at background station in the Pearl River Delta region. *Atmospheric Research*, **143**, 216–227, https://doi.org/10.1016/j.atmosres.2014.02.011.

Chen, Y. X., 2014: Analysis of aerosol types and sources in the typical pollution region of China based on MODIS product. M.S. thesis, Nanjing University of Information Science & Technology, 69 pp. (in Chinese with English abstract)

Gong, C. S., 2014: The preliminary research of aerosol climate effect by direct radiative forcing in different ecosystems in mainland China. PhD dissertation, Lanzhou University, 119pp. (in Chinese with English abstract)

Gong, C. S., J. Y. Xin, S. G. Wang, Y. S. Wang, P. C. Wang, L. L. Wang, and P. Li, 2014: The aerosol direct radiative forcing over the Beijing metropolitan area from 2004 to 2011. *Journal of Aerosol Science*, **69**, 62–70, https://doi.org/10.1016/j.jaerosci.2013.12.007.

Gong, C. S., J. Y. Xin, S. G. Wang, Y. S. Wang, and T. J. Zhang, 2017: Anthropogenic aerosol optical and radiative properties in the typical urban/suburban regions in China. *Atmospheric Research*, **197**, 177–187, https://doi.org/10.1016/j.atmosres.2017.07.002.

Guo, S., M. Hu, Z. B. Wang, J. Slanina, and Y. L. Zhao, 2010: Size-resolved aerosol water-soluble ionic compositions in the summer of Beijing: Implication of regional secondary formation. *Atmospheric Chemistry and Physics*, **10**(3), 947–959, https://doi.org/10.5194/acp-10-947-2010.

Hu, W. W., M. Hu, W. Hu, C. Chen, and J. F. Peng, 2016: Limitations of EC tracer method in areas with complicated primary sources. *Acta Scientiae Circumstantiae*, **36**(6), 2121–2130, https://doi.org/10.13671/j.hjkxxb.2015.0741. (in Chinese with English abstract)

Huan, N., L. M. Zeng, and M. Shao, 2005: Review of measurement techniques about organic carbon and elemental carbon in atmospheric particles. *Acta Scientiarum Naturalium Universitatis Pekinensis*, **41**(6), 957–964, https://doi.org/10.3321/j.issn:0479-8023.2005.06.017. (in Chinese with English abstract)

Huang, R. J., and Coauthors, 2014: High secondary aerosol contribution to particulate pollution during haze events in China. *Nature*, **514**(7521), 218–222, https://doi.org/10.1038/nature

13774.

Huang, X. J., 2016: Chemical and physical characteristics and source apportionment of atmospheric fine particles in typical cities of Beijing-Tianjin-Hebei region. PhD dissertation, University of Chinese Academy of Sciences, 137 pp. (in Chinese)

Huang, Y. M., Z. R. Liu, H. Chen, and Y. S. Wang, 2013: Characteristics of mass size distributions of water-soluble inorganic ions during summer and winter haze days of Beijing. *Environmental Science*, **34**(4), 1236–1244, https://doi.org/10.13227/j.hjkx.2013.04.017. (in Chinese with English abstract)

IPCC, 2014: *Climate Change 2013: the Physical Science Basis. Contribution of Working Group I to the Fifth Assessment Report of the Intergovernmental Panel on Climate Change*, Thomas et al., Eds., Cambridge University Press, New York.

Jacobson, M. Z., 2001: Strong radiative heating due to the mixing state of black carbon in atmospheric aerosols. *Nature*, **409**, 695–697, https://doi.org/10.1038/35055518.

Jacobson, M. Z., 2002: Control of fossil-fuel particulate black carbon and organic matter, possibly the most effective method of slowing global warming. *J. Geophys. Res. Atmos.*, **107**(D19), ACH 16-1–ACH 16-22, https://doi.org/10.1029/2001JD001376.

Jiang, N., Q. Li, F. C. Su, Q. Wang, X. Yu, P. R. Kang, R. Q. Zhang, and X. Y. Tang, 2018: Chemical characteristics and source apportionment of $PM_{2.5}$ between heavily polluted days and other days in Zhengzhou, China. *Journal of Environmental Sciences*, **66**, 188–198, https://doi.org/10.1016/j.jes.2017.05.006.

Jiang, R., 2017: Concentrations and pollution characteristics of organic carbon and elemental carbon in $PM_{2.5}$ during the heavy air pollution episodes in Nantong. *Environmental Protection Science*, **43**, 35–38, https://doi.org/10.16803/j.cnki.issn.1004-6216.2017.05.700. (in Chinese with English abstract)

Kaufman, Y. J., 1993: Aerosol optical thickness and atmospheric path radiance. *J. Geophys. Res. Atmos.*, **98**(D2), 2677–2692, https://doi.org/10.1029/92JD02427.

Kirkevåg, A., T. Iversen, and A. Dahlback, 1999: On radiative effects of black carbon and sulphate aerosols. *Atmos. Environ.*, **33**, 2621–2635, https://doi.org/10.1016/S1352-2310(98)00309-4.

Koepke P., J. Gasteiger, and M. Hess, 2015: Technical note: Optical properties of desert aerosol with non-spherical mineral particles: Data incorporated to OPAC. *Atmospheric Chemistry and Physics*, **15**, 5947–5956, https://doi.org/10.5194/acp-15-5947-2015.

Kong, L. B., J. Y. Xin, Z. R. Liu, K. Q. Zhang, G. Q. Tang, W. Y. Zhang, and Y. S. Wang, 2017: The $PM_{2.5}$ threshold for aerosol extinction in the Beijing megacity. *Atmos. Environ.*, **167**, 458–465, https://doi.org/10.1016/j.atmosenv.2017.08.047.

Kong, S. F., and Coauthors, 2014: Ion chemistry for atmospheric size-segregated aerosol and depositions at an offshore site of Yangtze River Delta region, China. *Atmospheric Research*, **147–148**, 205–226, https://doi.org/10.1016/j.atmosres.2014.05.018.

Koo, J. H., and Coauthors, 2016: Wavelength dependence of Ångström exponent and single scattering albedo observed by skyradiometer in Seoul, Korea. *Atmospheric Research*, **181**, 12–19, https://doi.org/10.1016/j.atmosres.2016.06.006.

Li, S., W. J. Wang, B. L. Zhang, and Y. Han, 2009: Indirect radiative forcing and climatic effect of the anthropogenic nitrate aerosol on regional climate of China. *Adv. Atmos. Sci.*, **26**, 543–552, https://doi.org/10.1007/s00376-009-0543-9.

Logan, T., B. K. Xi, X. Q. Dong, Z. Li, and M. Cribb, 2013: Classification and investigation of Asian aerosol absorptive properties. *Atmospheric Chemistry and Physics*, **13**(4), 2253–2265, https://doi.org/10.5194/acp-13-2253-2013.

Logan, T., B. K. Xi, and X. Q. Dong, 2014: Aerosol properties and their influences on marine boundary layer cloud condensation nuclei at the ARM mobile facility over the Azores. *J. Geophys. Res. Atmos.*, **119**(8), 4859–4872, https://doi.org/10.1002/2013JD021288.

Lohmann, U., and J. Feichter, 2005: Global indirect aerosol effects: A review. *Atmospheric Chemistry and Physics*, **5**, 715–737, https://doi.org/10.5194/acp-5-715-2005.

Ma, Y. J., J. Y. Xin, W. Y. Zhang, and Y. S. Wang, 2016: Optical properties of aerosols over a tropical rain forest in Xishuangbanna, South Asia. *Atmospheric Research*, **178–179**, 187–195, https://doi.org/10.1016/j.atmosres.2016.04.004.

Mukai, S., I. Sano, M. Satoh, and B. N. Holben, 2006: Aerosol properties and air pollutants over an urban area. *Atmospheric Research*, **82**, 643–651, https://doi.org/10.1016/j.atmosres.2006.02.020.

Palancar, G. G., L. E. Olcese, M. Achad, M. L. López, and B. M. Toselli, 2017: A long term study of the relations between erythemal UV-B irradiance, total ozone column, and aerosol optical depth at central Argentina. *Journal of Quantitative Spectroscopy and Radiative Transfer*, **198**, 40–47, https://doi.org/10.1016/j.jqsrt.2017.05.002.

Pio, C., and Coauthors, 2011: OC/EC ratio observations in Europe: Re-thinking the approach for apportionment between primary and secondary organic carbon. *Atmos. Environ.*, **45**, 6121–6132, https://doi.org/10.1016/j.atmosenv.2011.08.045.

Qian, Y., H. Q. Wang, C. B. Fu, and Z. F. Wang, 1998: Seasonal and spatial variation of radiative effects of anthropogenic sulfate aerosol. *Adv. Atmos. Sci.*, **15**, 380–392, https://doi.org/10.1007/s00376-998-0008-6.

Ram, K., and M. M. Sarin, 2010: Spatio-temporal variability in atmospheric abundances of EC, OC and WSOC over Northern India. *Journal of Aerosol Science*, **41**, 88–98, https://doi.org/10.1016/j.jaerosci.2009.11.004.

Ram, K., S. Singh, M. M. Sarin, A. K. Srivastava, and S. N. Tripathi, 2016: Variability in aerosol optical properties over an urban site, Kanpur, in the Indo-Gangetic Plain: A case study of haze and dust events. *Atmospheric Research*, **174–175**, 52–61, https://doi.org/10.1016/j.atmosres.2016.01.014.

Reisen, F., C. P. Meyer, and M. D. Keywood, 2013: Impact of biomass burning sources on seasonal aerosol air quality. *Atmos. Environ.*, **67**, 437–447, https://doi.org/10.1016/j.atmosenv.2012.11.004.

Russell, A. G., G. J. McRae, and G. R. Cass, 1983: Mathematical modeling of the formation and transport of ammonium nitrate aerosol. *Atmos. Environ.*, **17**, 949–964, https://doi.org/10.1016/0004-6981(83)90247-0.

Seinfeld, J. H., and S. N. Pandis, 1998: *Atmospheric Chemistry and Physics: from Air Pollution to Climate Change*. Wiley.

Shao, P., J. Y. Xin, J. L. An, L. B. Kong, B. Y. Wang, J. X. Wang, Y. S. Wang, and D. Wu, 2017: The empirical relationship between $PM_{2.5}$ and AOD in Nanjing of the Yangtze River Delta. *Atmospheric Pollution Research*, **8**(2),

233–243, https://doi.org/10.1016/j.apr.2016.09.001.

Sheng, P. X., J. T. Mao, J. G. Li, Z. M. Ge, A. C. Zhang, J. G. Sang, N. X. Pan, and H. S. Zhang, 2013: *Atmospheric Physic*. Peking University Press, 551 pp. (in Chinese)

Singh, A., and S. Dey, 2012: Influence of aerosol composition on visibility in megacity Delhi. *Atmos. Environ.*, **62**, 367–373, https://doi.org/10.1016/j.atmosenv.2012.08.048.

Srinivas, B., and M. M. Sarin, 2014: $PM_{2.5}$, EC and OC in atmospheric outflow from the Indo-Gangetic plain: Temporal variability and aerosol organic carbon-to-organic mass conversion factor. *Science of the Total Environment*, **487**, 196–205, https://doi.org/10.1016/j.scitotenv.2014.04.002.

Su, H. J., and Coauthors, 2018: Effects of transport on aerosols over the eastern slope of the Tibetan Plateau: Synergistic contribution of Southeast Asia and the Sichuan Basin. *Atmos. Ocean. Sci. Lett.*, **11**(5), 425–431, https://doi.org/10.1080/16742834.2018.1512832.

Su, H. J., 2018: Observation and extinction characteristics of $PM_{2.5}$ in typical urban areas of North China. M.S. thesis, Chengdu University of Information Technology. (in Chinese with English abstract)

Tang, B. Y., and Coauthors, 2018: Characteristics of complex air pollution in typical cities of North China. *Atmos. Ocean. Sci. Lett.*, **11**(1), 29–36, https://doi.org/10.1080/16742834.2018.1394158.

Tian, H. W., Y. F. Zheng, H. L. Chen, W. Deng, and Z. X. Du, 2010: Inversion and analysis of aerosol optical depth in Zhengzhou. *Meteorological Science and Technology*, **38**(4), 515–520, https://doi.org/10.3969/j.issn.1671-6345.2010.04.023. (in Chinese with English abstract)

Tian, S. L., Y. P. Pan, and Y. S. Wang, 2016: Size-resolved source apportionment of particulate matter in urban Beijing during haze and non-haze episodes. *Atmospheric Chemistry and Physics*, **16**, 1–19, https://doi.org/10.5194/acp-16-1-2016.

Wang, L. C., W. Gong, X. G. Xia, J. Zhu, J. Li, and Z. M. Zhu, 2015: Long-term observations of aerosol optical properties at Wuhan, an urban site in Central China. *Atmos. Environ.*, **101**, 94–102, https://doi.org/10.1016/j.atmosenv.2014.11.021.

Wang, M. X., R. J. Zhang, and Y. F. Pu, 2001: Recent researches on aerosol in China. *Adv. Atmos. Sci.*, **18**(4), 576–586, https://doi.org/10.1007/s00376-001-0046-9.

Wang, P., H. Z. Che, X. C. Zhang, Q. L. Song, Y. Q. Wang, Z. H. Zhang, X. Dai, and D. J. Yu, 2010: Aerosol optical properties of regional background atmosphere in Northeast China. *Atmos. Environ.*, **44**, 4404–4412, https://doi.org/10.1016/j.atmosenv.2010.07.043.

Wang, T., 2016: Research on the spatial and temporal distribution of $PM_{2.5}$ in Changsha, Zhuzhou and Xiangtan. M.S. thesis, Hunan University of Science and Technology, 79 pp. (in Chinese with English abstract)

Wang, Y. Q., X. Y. Zhang, and R. R. Draxler, 2009: TrajStat: GIS-based software that uses various trajectory statistical analysis methods to identify potential sources from long-term air pollution measurement data. *Environmental Modelling & Software*, **24**, 938–939, https://doi.org/10.1016/j.envsoft.2009.01.004.

Watson, J. G., J. C. Chow, F. W. Lurmann, and S. P. Musarra, 1994: Ammonium nitrate, nitric acid, and ammonia equilibrium in wintertime Phoenix, Arizona. *Air & Waste*, **44**(4), 405–412, https://doi.org/10.1080/1073161X.1994.10467262.

Xia, X. G., H. B. Chen, P. Goloub, X. M. Zong, W. X. Zhang, and P. C. Wang, 2013: Climatological aspects of aerosol optical properties in north china plain based on ground and satellite remote-sensing data. *Journal of Quantitative Spectroscopy and Radiative Transfer*, **127**, 12–23, https://doi.org/10.1016/j.jqsrt.2013.06.024.

Xin, J. Y., and Coauthors, 2007: Aerosol optical depth (AOD) and Ångström exponent of aerosols observed by the Chinese Sun Hazemeter Network from August 2004 to September 2005. *J. Geophys. Res. Atmos.*, **112**(D5), D05203, https://doi.org/10.1029/2006JD007075.

Xin, J. Y., and Coauthors, 2015: The campaign on atmospheric aerosol research network of China: CARE-China. *Bull. Amer. Meteor. Soc.*, **96**(7), 1137–1155, https://doi.org/10.1175/BAMS-D-14-00039.1.

Xin, J. Y., and Coauthors, 2016a: The observation-based relationships between $PM_{2.5}$ and AOD over China. *J. Geophys. Res. Atmos.*, **121**, 10 701–10 716, https://doi.org/10.1002/2015JD024655.

Xin, J. Y., C. S. Gong, S. G. Wang, and Y. S. Wang, 2016b: Aerosol direct radiative forcing in desert and semi-desert regions of northwestern China. *Atmospheric Research*, **171**, 56–65, https://doi.org/10.1016/j.atmosres.2015.12.004.

Xu, G. J., Y. Gao, Q. Lin, W. Li and L. Q. Chen, 2013: Characteristics of water-soluble inorganic and organic ions in aerosols over the Southern Ocean and coastal East Antarctica during austral summer. *J. Geophys. Res. Atmos.*, **118**, 13 303–13 318, https://doi.org/10.1002/2013JD019496.

Zhang, C. X., and Coauthors, 2019: Satellite UV-Vis spectroscopy: Implications for air quality trends and their driving forces in China during 2005–2017. *Light, Science & Applications*, **8**, 100, https://doi.org/10.1038/s41377-019-0210-6.

Zhang, F., Z. W. Wang, H. R. Cheng, X. P. Lv, W. Gong, X. M. Wang, and G. Zhang, 2015: Seasonal variations and chemical characteristics of $PM_{2.5}$ in Wuhan, central China. *Science of the Total Environment*, **518–519**, 97–105, https://doi.org/10.1016/j.scitotenv.2015.02.054.

Zhang, J. H., J. T. Mao, and M. H. Wang, 2002: Analysis of the aerosol extinction characteristics in different areas of China. *Adv. Atmos. Sci.*, **19**(1), 136–152, https://doi.org/10.1007/s00376-002-0040-x.

Zhang, K. Q., and Coauthors, 2018: The aerosol optical properties and $PM_{2.5}$ components over the world's largest industrial zone in Tangshan, North China. *Atmospheric Research*, **201**, 226–234, https://doi.org/10.1016/j.atmosres.2017.10.025.

Zhang, K., Y. S. Wang, T. X. Wen, G. R. Liu, B. Hu, and Y. N. Zhao, 2008: On-line analysis and mass concentration characters of the Alkali Metal Ions of PM_{10} in Beijing. *Environmental Science*, **29**(1), 246–252, https://doi.org/10.3321/j.issn:0250-3301.2008.01.041. (in Chinese with English abstract)

Zhang, T. H., and H. Liao, 2016: Aerosol absorption optical depth of fine-mode mineral dust in eastern China. *Atmos. Ocean. Sci. Lett.*, **9**(1), 7–14, https://doi.org/10.1080/16742834.2015.1126154.

Zhang, X. Y., Y. Q. Wang, T. Niu, X. C. Zhang, S. L. Gong, Y. M. Zhang, and J. Y. Sun, 2012: Atmospheric aerosol compositions in China: Spatial/temporal variability, chemical signature, regional haze distribution and comparisons with global aerosols. *Atmospheric Chemistry and Physics*, **12**, 779–799, https://doi.org/10.5194/acp-12-779-2012.

Zhao, D. D., J. Y. Xin, C. S. Gong, X. Wang, Y. J. Ma, and Y. N. Ma, 2018: Trends of aerosol optical properties over the heavy industrial zone of northeastern Asia in the past decade (2004-2015). *J. Atmos. Sci.*, **75**(6), 1741–1754, https://doi.org/10.1175/JAS-D-17-0260.1.

Zhao, H. J., and Coauthors, 2013b: Aerosol optical properties over urban and industrial region of Northeast China by using ground-based sun-photometer measurement. *Atmos. Environ.*, **75**, 270–278, https://doi.org/10.1016/j.atmosenv.2013.04.048.

Zhao, H. J., H. Z. Che, Y. J. Ma, X. G. Xia, Y. F. Wang, P. Wang, and X. C. Wu, 2015: Temporal variability of the visibility, particulate matter mass concentration and aerosol optical properties over an urban site in Northeast China. *Atmospheric Research*, **166**, 204–212, https://doi.org/10.1016/j.atmosres.2015.07.003.

Zhao, P. S., F. Dong, D. He, X. J. Zhao, X. L. Zhang, W. Z. Zhang, Q. Yao, and H. Y. Li, 2013a: Characteristics of concentrations and chemical compositions for $PM_{2.5}$ in the region of Beijing, Tianjin, and Hebei, China. *Atmospheric Chemistry and Physics*, **13**, 4631–4644, https://doi.org/10.5194/acp-13-4631-2013.

Zheng, X. Y., X. D. Liu, F. H. Zhao, F. K. Duan, T. Yu, and H. Cachier, 2005: Seasonal characteristics of biomass burning contribution to Beijing aerosol. *Science in China Series B: Chemistry*, **48**(5), 481–488, https://doi.org/10.1360/042005-15.